THESIS REPORT

Master's Degree

Analysis and Evaluation of a Shell Finite Element with Drilling Degree of Freedom

by L. Jin
Advisor: M.A. Austin

M.S. 94-12

ISR
INSTITUTE FOR SYSTEMS RESEARCH

ABSTRACT

Title of Thesis:	Analysis and Evaluation of a Shell Finite Element with Drilling Degree of Freedom
Name of degree candidate:	Lanheng Jin Department of Civil Engineering and Institute for System Research University of Maryland at College Park
Degree and Year:	Master of Science, 1994
Thesis directed by:	Dr. Mark A. Austin Associate Professor Department of Civil Engineering and Institute for System Research University of Maryland at College Park

A flat shell finite element is obtained by superposing plate bending and membrane components. Normally, shell elements of this type possess five degrees of freedom (DOF), three displacement DOF, u, v and w, and two in-plane rotation DOF, θ_x and θ_y, at each node. A sixth degree of freedom, θ_z, is associated with the shell normal rotation, and is not usually required by the theory. In practice, however, computational and modeling problems can be caused by a failure to include this degree of freedom in finite element models.

This paper presents the formulation and testing of a four node quadrilateral

thin flat shell finite element, which has six DOF per node. The sixth DOF is obtained by combining by a membrane element with a normal rotation θ_z, the so-called the drilling degree of freedom, and a discrete Kirchhoff plate element. The flat shell has a 24×24 element stiffness matrix. Numerical examples are given for (a) shear-loaded cantilever beam, (b) square plate, (c) cantilever I-beam and (d) folded plate. Performance of the flat shell finite element is also compared to a four node flat shell element in ANSYS-5.0 in case studies (a)-(d), and a quadrilateral flat shell element from SAP-90 in case study (c).

DEDICATION

For my parents and Aoyasuly.

ACKNOWLEDGMENTS

I would like to sincerely thank my advisor, Professor Mark A. Austin, for his vision, guidance and patience during this project. This work would not have been possible without the assistance of Professor R. L. Taylor, University of California at Berkeley, who provided help and encouragement to pursue this project. My appreciations go also to Professor Peter Chang, who reviewed the thesis carefully and offered important comments.

In addition, I wish to take this opportunity to thank all of the students, faculty and staff of the Institute for Systems Research for their continued support and encouragement.

TABLE OF CONTENTS

LIST OF TABLES

LIST OF FIGURES

CHAPTER
1

Introduction

This thesis describes the formulation and testing of a four node quadrilateral flat shell finite element that incorporates membrane and bending components of displacement; each node is modeled with three displacement and three rotation degrees of freedom. Many engineering structures are composed of flat surfaces at least in part, and these can be simply reproduced. Shell structures with an arbitrary curved shape are modeled as an assembly of small-size flat shell elements. As the size of the flat elements decreases, convergence of the element behavior occurs. The mathematics of convergence was first discussed in 1977 by Ciarlet [8]. Numerical experiments have subsequently shown that excellent results can be obtained with the flat shell element (Chapter 3 in [26] and Chapter 13 in [27]).

In small displacement models of flat shell elements, the effects of membrane and bending strain are not coupled in the energy expression within the elements. Coupling occurs only on the interelement boundary. Therefore, we consider a flat shell element as combination of a plane stress element and a plate bending element. In the combined element subject to membrane and bending actions, the displacements prescribed for 'in-plane' forces do not affect the bending de-

formations, and vice versa.

1.1 Objectives and Scope

The purpose of this chapter is to introduce and describe analytical formulations for flat shell finite elements that combine plane stress element with plate bending element. Background material is provided for development of the membrane component of the flat shell element.

Sections 1.2 and 1.3 describe the classical formulation of flat shell elements without a normal rotation θ_z (i.e. the shell finite element is modeled with three nodal displacement parameters, u, v and w, and two rotation parameters, θ_x and θ_y, parallel to the plane of the plate at each node). And then, the membrane component including the vertex rotation perpendicular to the plane of the plate is introduced. As the part of plane membrane action, this membrane component may be used to consist in flat shell elements by regular method described in Section 1.2.

Chapters 2 and 3 will describe details of a membrane element formulated with drilling degree of freedom, and a bending component based upon Kirchhoff assumptions of flat shell finite elements. Numerical experiments with the shell finite element are presented in Chapter 4.

1.2 Classical Flat Shell Element

In classical formulations of flat shell element that combine plane stress element with plate bending element [26, 27], we know that for plane stress actions, the state of strain is uniquely described in terms of the u and v displacements at

each typical node i. These modeling assumptions are shown in Figure 1.1. A

a). *Plane Membrane Actions and Deformations*

b). *Bending Actions and Deformations*
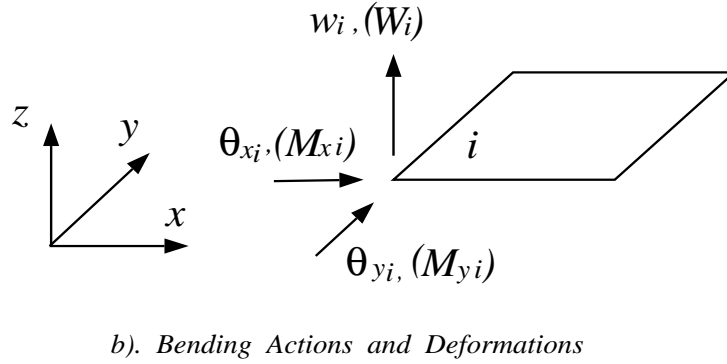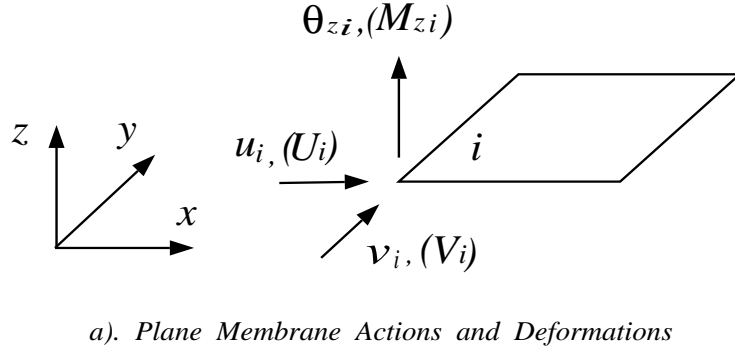
Figure 1.1: A flat shell element subject to plane membrane and bending action.

right-handed coordinate frame is employed. We use the variables u and v for in-plane displacements along the x and y axes respectively, the variable w for displacements perpendicular to the plane of the shell element, and the variables θ_x, θ_y and θ_z for clockwise rotations about the x, y and z axes.

By minimizing total potential energy, the classical formulation leads to a stiffness matrix $[K^p]$, nodal forces $\{f^p\}$, and element displacement $\{q^p\}$, where

$$\{f^p\} = [K^p]\{q^p\} \tag{1.2.1}$$

with $\quad \{q_i^p\} = \left\{ \begin{array}{c} u_i \\ \\ v_i \end{array} \right\} \quad$ and $\quad \{f_i^p\} = \left\{ \begin{array}{c} U_i \\ \\ V_i \end{array} \right\}, \quad$ for $i = 1, 2, 3, 4.$

Here we use the superscript 'p' to denote in-plane deformation of the shell element. Similarly, when bending action is considered, the state of strain is given uniquely by the nodal displacements in the z direction, w, and the two rotations θ_x and θ_y. The result is bending stiffness matrices of the type

$$\{f^b\} = [K^b]\{q^b\}, \tag{1.2.2}$$

where $\quad \{q_i^b\} = \left\{ \begin{array}{c} w_i \\ \theta_{xi} \\ \theta_{yi} \end{array} \right\} \quad$ and $\quad \{f_i^b\} = \left\{ \begin{array}{c} W_i \\ M_{xi} \\ M_{yi} \end{array} \right\}, \quad$ for $i = 1, 2, 3, 4.$

The superscript 'b' is introduced to denote bending deformation of the shell element. Notice that in the classical formulation, the rotation of the normal to the surface of the flat shell, given by θ_z, is not included in the definition of deformations as a parameter of nodes in membrane mode. Instead, we take this rotation parameter into account by introducing a fictitious couple M_z, and inserting zeros at appropriate positions in the element stiffness matrices. The combined nodal displacements are now given by

$$\{q_i\} \quad = \quad \{u_i, v_i, w_i, \theta_{xi}, \theta_{yi}, \theta_{zi}\}^T$$

$$= \{<q_i^p>, <q_i^b>, \theta_{zi}\}^T, \tag{1.2.3}$$

and the appropriate general forces as

$$
\begin{aligned}
\{f_i\} &= \{U_i, V_i, W_i, M_{xi}, M_{yi}, M_{zi}\}^T \\
&= \{<f_i^p>, <f_i^b>, M_{zi}\}^T, \tag{1.2.4}
\end{aligned}
$$

where $<q_i^p>$, $<q_i^b>$, $<f_i^p>$ and $<f_i^b>$ are defined as equations (1.2.1) and (1.2.2). For a flat shell element we write

$$\{f\} = [K]\{q\} \tag{1.2.5}$$

with $[K^p] = [K_{rs}^p]$ and $[K^b] = [K_{rs}^b]$,   where subscripts r represents row number and s does column number of submatrices.

$$
[K_{rs}] =
\begin{bmatrix}
K_{rs}^p & & 0 & 0 & 0 & 0 \\
 & & 0 & 0 & 0 & 0 \\
0 & 0 & & & & 0 \\
0 & 0 & & K_{rs}^b & & 0 \\
0 & 0 & & & & 0 \\
0 & 0 & 0 & 0 & 0 & 0
\end{bmatrix}
\tag{1.2.6}
$$

Felippa [6] reports that Turner et al. [25] and Taig [21] have used this approach to modeling to develop membrane components of rectangular and

5

Figure 1.2: Slabs and columns building.

quadrilateral flat shell elements, respectively. Numerical experiments have been conducted to assess the performance of these membrane elements – one such experiment is the computation of in-plane bending behavior for a thin rectangular shear-loaded cantilever beam. The numerical experiments reveal that these membrane elements are excessively stiff. Figure 1.2 shows a second application area where floor slabs in a building are supported by columns. In the real building structure, the columns will be firmly attached to the floor slabs. Hence, if the floor slab rotates due to external loadings, compatibility requires that the columns rotate about their axis by the same amount. Use of the abovementioned shell element (i.e. five degrees of freedom per node) for this application is inappropriate because the finite element model does not have a rotational degree of freedom perpendicular to the plane of the floor. As such, the column torsional stiffness cannot be connected to the shell element stiffness [10, 11]. Figure 1.3 shows what will happen in the mathematical model. The column will displace

in the translational degrees of freedom, but may not rotate by the same amount as the shell. This problem of incompatible displacements can be overcome with the formulation of shell finite elements having six degrees of freedom per node.
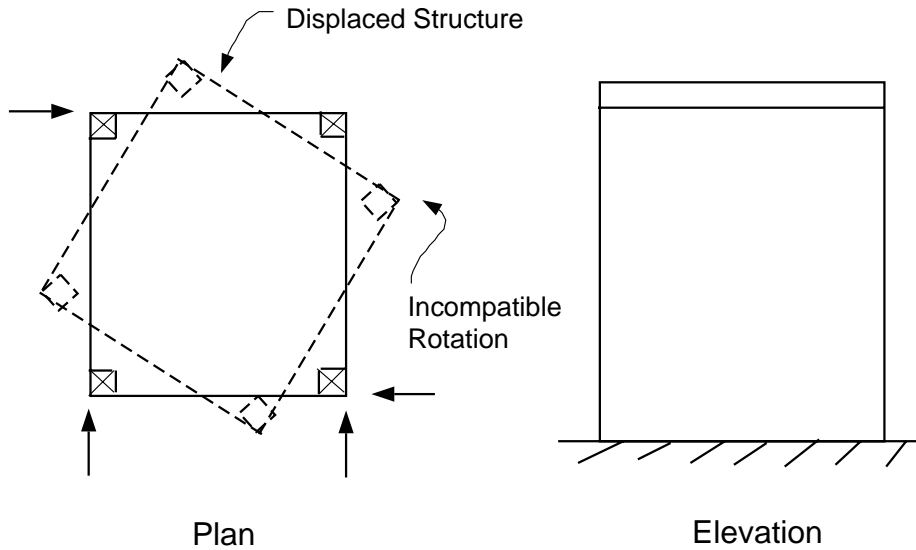
Figure 1.3: Finite element model of simple table using shell element having only five degree of freedom per node.

Programming difficulties (i.e. zero stiffness in the θ_{zi} direction; equations of the flat shell elements do not include rotational parameter) with this class of elements occur when elements meeting at a node are coplanar or nearly coplanar. Two applications are modeling of flat or folded shell segments, and modeling of straight boundaries of cylindrical shaped shells [26, 27, 10]. When the local coordinate directions of these elements happens to coincide with the global ones, the equilibrium equations reduce to $0 = 0$, a true but useless component of modeling information. If, on the other hand, the local and global coordinate directions differ, and a transformation is accomplished, then the global stiffness matrix is singular. Detection of this singularity is difficult. There are two simple

procedures for solving this problem:

(a) Assembling the stiffness matrices of elements at points where the elements are coplanar in local coordinates and deleting the equation $0 = 0$.

(b) Inserting an arbitrary coefficient $K'_{\theta z}$ at points where the elements are coplanar only.

The second procedure leads to the replacement of equation $0 = 0$ by an equation $K'_{\theta z}\theta_{zi} = 0$ in the local coordinates. A perfectly well-behaved global stiffness matrix is achieved after a local-to-global coordinate transformation, and all displacements, now including θ_{zi}, can be calculated. Since θ_{zi} does not affect the stresses, and indeed, is uncoupled from all others equilibrium equations, any non-zero value of $K'_{\theta z}$ can be inserted as an external stiffness without affecting the results. Both of these approaches lead to implementation difficulties because a decision on the coplanar nature of the shell elements is necessary.

The aforementioned modeling and programming difficulties can be avoided by using higher-order displacement nodes linked with corner rotations normal to the plane of the element. These are the so-called drilling degree of freedom [6].

1.3 Compatible Membrane Element Including Vertex Rotations

The difficulties described in Section 1.1 vanish when nodal rotational parameters normal to the element plane are added. Progress in this direction was first made by Allman [1], who introduced the concept of the 'vertex rotation', ω, and Cook [9] who gave a geometrical interpolation of the vertex rotation, w, in

relation to the mid-side node transverse displacement of quadratic elements.

Consider a element side of length l, as shown in Figure 1.4. The edge-tangent
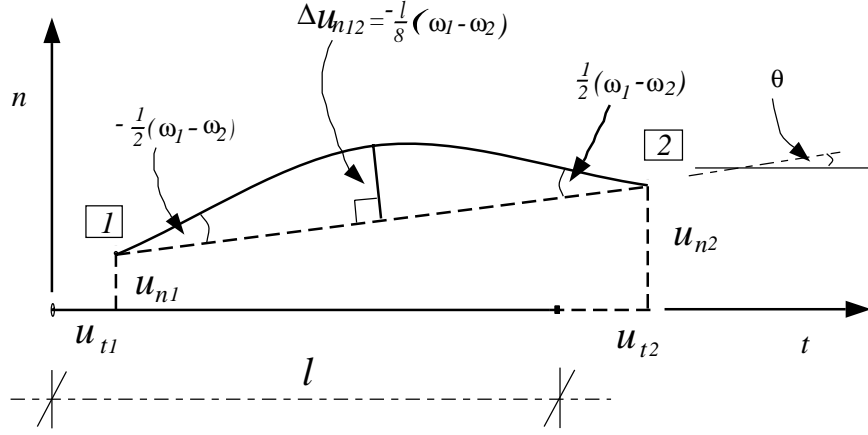
Figure 1.4: Displacement of an element side "1", "2".

displacement u_t is interpolated linearly in the edge-tangent coordinate s, as

$$u_t = (1 - \frac{s}{l})u_{t_1} + \frac{s}{l}u_{t_2} \tag{1.3.1}$$

and the edge-normal displacement u_n is interpolated quadratically, as

$$u_n = (1 - \frac{s}{l})u_{n_1} + \frac{s}{l}u_{n_2} + 4\frac{s}{l}(1 - \frac{s}{l})\Delta u_{n_{12}} \tag{1.3.2}$$

where $\Delta u_{n_{12}}$ is hierarchical displacement (relative to the 4-node interpolation values). From Figure 1.4 we observe that $\theta = (u_{n_2} - u_{n_1})/l$. Differentiating

9

equations (1.3.2) gives

$$
\begin{aligned}
\frac{\partial u_n}{\partial s} &= -\frac{u_{n_1}}{l} + \frac{u_{n_2}}{l} + \frac{4}{l}(1 - \frac{2s}{l})\Delta u_{n_{12}} \\
&= \theta + \frac{4}{l}(1 - \frac{2s}{l})\Delta u_{n_{12}} \tag{1.3.3}
\end{aligned}
$$

According to Allman [1, 10], the definition of the vertex rotation, ω, is

$$
-\omega_2 + \omega_1 = \frac{\partial u_n}{\partial s}\Big|_l - \frac{\partial u_n}{\partial s}\Big|_0 \tag{1.3.4}
$$

where ω_1 and ω_2 are the vertex rotations at nodes 1 and 2, respectively. Since

$$
\frac{\partial u_n}{\partial s}\Big|_0 = \theta + \frac{4}{l}\Delta u_{n_{12}}
$$

$$
\frac{\partial u_n}{\partial s}\Big|_l = \theta - \frac{4}{l}\Delta u_{n_{12}} \tag{1.3.5}
$$

therefore

$$
\omega_1 - \omega_2 = -\frac{8}{l}\Delta u_{n_{12}}. \tag{1.3.6}
$$

Also, we get

$$
\Delta u_{n_{12}} = -\frac{l}{8}(\omega_1 - \omega_2) \tag{1.3.7}
$$

$$
\frac{\partial u_n}{\partial s}\Big|_0 - \theta = -\frac{1}{2}(\omega_1 - \omega_2) \tag{1.3.8}
$$

10

$$\frac{\partial u_n}{\partial s}\Big|_l - \theta = \frac{1}{2}(\omega_1 - \omega_2) \tag{1.3.9}$$

where ω_1 and ω_2 are the so-called vertex rotation parameters at nodes 1 and 2, respectively. Now we can rewrite the interpolation of u_n as

$$u_n = (1 - \frac{s}{l})u_{n_1} + \frac{s}{l}u_{n_2} - \frac{s}{2}(1 - \frac{s}{l})(\omega_1 - \omega_2) \tag{1.3.10}$$

Expressions for displacements at the element boundary, u and v, in terms of the nodal parameters along the edge of the element (i.e. two nodal translation quantities, u_i and v_i, and one vertex rotation quantity, ω_i) are obtained through u_t (i.e. equation (1.3.1)) and coordinate transformations of directions between the systems x-y and n-t. A schematic of the required coordinate transformation is shown in Figure 1.5. The transformation matrices are

$$\begin{Bmatrix} u_n \\ u_t \end{Bmatrix} = \begin{bmatrix} C & S \\ -S & C \end{bmatrix} \begin{Bmatrix} u \\ v \end{Bmatrix}, \tag{1.3.11}$$

and

$$\begin{Bmatrix} u \\ v \end{Bmatrix} = \begin{bmatrix} C & -S \\ S & C \end{bmatrix} \begin{Bmatrix} u_n \\ u_t \end{Bmatrix}, \tag{1.3.12}$$

where $C = \cos(\gamma)$ and $S = \sin(\gamma)$. γ is the angle between the outward normal direction to the element side and the x-axis. We can use a similar technique to

11
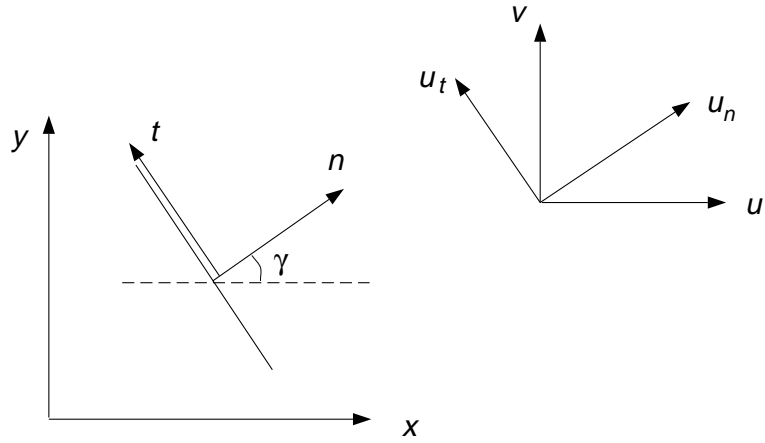
Figure 1.5: Coordinate transformation of directions between systems x-y and n-t.

obtain boundary displacements u and v in terms of the nodal parameters u_i, v_i and ω_i, along other all edges of elements at the boundary,

$$u = u(u_i, v_i, \omega_i)$$
$$v = v(u_i, v_i, \omega_i)$$

$$(1.3.13)$$

where u and v are the Cartesian components of boundary displacements and u_i, v_i and ω_i, the Cartesian components of nodal parameters.

With the coordinate transformation in plane, we can now write the quadratic displacement interpolation fields inside the entire element, u and v, in terms of nodal and mid-side displacement parameters. They are:

$$u = \sum_{i=1}^{8} N_i(\xi, \eta) u_i \qquad (1.3.14)$$

and

$$v = \sum_{i=1}^{8} N_i(\xi, \eta) v_i \tag{1.3.15}$$

In equations (1.3.14) and (1.3.15), ξ and η are parametric coordinates [27], and $N_i(\xi, \eta)$ are shape functions of the 8-node Serendipity element [26]. The shape functions are

$$N_i = \frac{1}{2}(1 - \xi^2)(1 + \eta_i\eta), \qquad i = 5, 7$$

$$N_i = \frac{1}{2}(1 - \eta^2)(1 + \xi_i\xi), \qquad i = 6, 8$$

$$N_i = \frac{1}{4}(1 + \xi_i\xi)(1 + \eta_i\eta) - \frac{1}{2}N_m - \frac{1}{2}N_n$$

$$i = 1, 2, 3, 4, \qquad m, n = 8, 5; 5, 6; 6, 7; 7, 8; \tag{1.3.16}$$

u_i and v_i as $i = 1, 2, 3, 4$ are nodal displacement parameters, and u_i and v_i as $i = 5, 6, 7, 8$ are mid-side displacement parameters. Finally, the quadratic displacement interpolation fields u and v within the entire element may be described in terms of all nodal parameters, u_i, v_i and ω_i ($i = 1, 2, 3, 4$) by substituting the expressions for u and v interpolations in the boundaries, (i.e. equations (1.3.13)), which are the expressions of mid-side displacement parameters, u_i and v_i ($i = 5, 6, 7, 8$) in terms of the nodal parameters, u_i, v_i and ω_i ($i = 1, 2, 3, 4$) into the quadratic interpolation fields of the entire element with mid-side displacement values, equation (1.3.14) and (1.3.15).

The element is compatible because of the quadratic interpolation with ver-

tex rotations parameters ω_1 and ω_2 in the boundary. In general, however, the element based on the ω connector will have a defect. The new nodal connector is not equal to the *true* rotations at nodes, even though it can be related to it. For this reason, it is concluded that a better way is to use the true rotations, so-called the drilling degree of freedom at nodes, as nodal rotational parameters [10, 16].

CHAPTER

2

Membrane Part of Flat Shell Element

In this chapter we derive a flat shell finite element model that contains nodal drilling degree of freedom. We demonstrate that this approach to modeling leads to a class of finite elements that performs better than those element mentioned in Section 1.2. For a summary of the literature on drilling degree of freedom approximations, see references [2, 3, 26, 27, 10, 20] and [16].

Unlike the definition of the vertex rotation ω given in equation (1.3.4), the drilling degree of freedom is defined as

$$\Phi = \frac{1}{2}(\frac{\partial v}{\partial x} - \frac{\partial u}{\partial y}). \qquad (2.0.1)$$

The drilling degree of freedom may be physically interpreted as a true rotation of the vertex bisecting the angle between adjacent edges of the finite element. A schematic of the angle bisector and associated partial derivatives in element displacements is shown in Figure 2.1.

This chapter discusses two approaches for producing the so-called drilling degree of freedom. The first approach was first reported by Sabir in 1985 [20]. He used strain-assumptions to develop a class of non-conforming elements, which
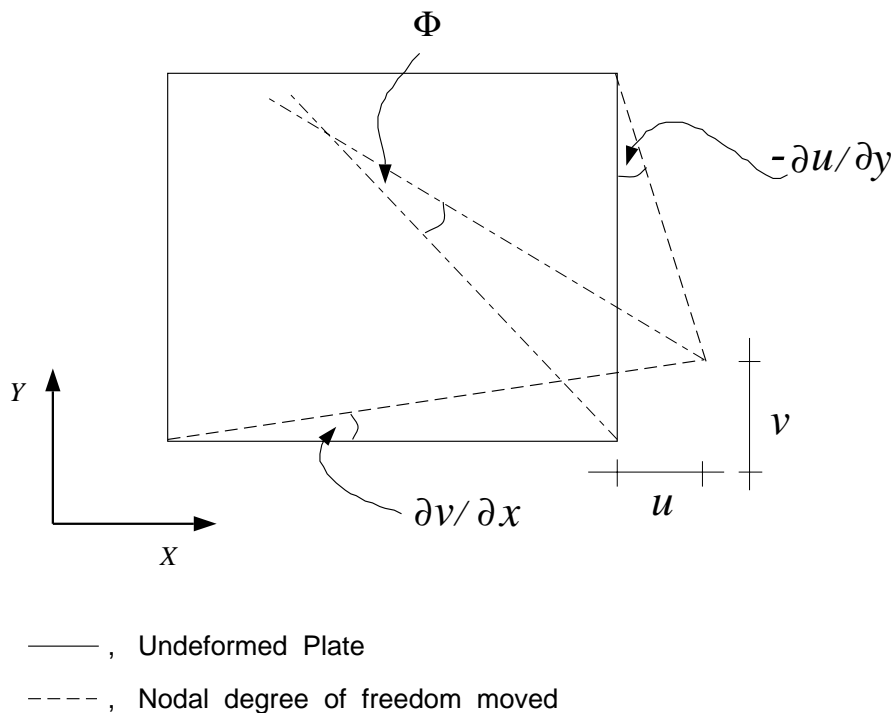
Figure 2.1: Physical interpretation of the drilling degree of freedom.

unfortunately suffer from geometrical restrictions and zero energy modes [10]. In fact, numerical experiments indicate that only rectangular elements are well behaved, and provide accurate results [10]. The second approach, as presented by Ibrahimbegovic et al. in 1990 [14], adopts a variational formulation, initially suggested by Hughes and Brezzi [11, 12]. The latter approach employs an independent rotation field to achieve quadrilateral flat shell elements that incorporate bending with a high order of accuracy. Details of theoretical formulation are presented in Chapter 3. In Chapter 4 we will conduct numerical experiments, and show that these elements exhibit excellent accuracy.

2.1 Sabir's rectangular membrane element with drilling degree of freedom based on the strain approach

Based on the strain analysis, Sabir derived [20] a rectangular membrane element with drilling degree of freedom, as defined in equation (2.0.1). A brief description follows. From the strain-displacement relationship in-plane elasticity, I can write

$$\begin{cases} \varepsilon_x = \partial u / \partial x \\ \varepsilon_y = \partial v / \partial y \\ \varepsilon_{xy} = \partial u / \partial y + \partial v / \partial x \end{cases} \tag{2.1.1}$$

If $\varepsilon_x = \varepsilon_y = \varepsilon_{xy} = 0$, then the equations above can be integrated to obtain

$$\begin{cases} u = a_1 - a_3 y \\ v = a_2 + a_3 x \end{cases} \tag{2.1.2}$$

Notice that equations (2.1.2) are described in terms of three components; a_1 and a_2 are the translational components, and a_3 the inplane rotation. Together a_1, a_2 and a_3 represent rigid body displacements.

Now let's consider the shape functions needed model displacements in a four node quadrilateral finite elements. If each node has three degrees of freedom — two translational degrees of freedom and one rotational degree of freedom — then the shape functions should contain twelve independent constants. Having used three of these in the representation of the rigid body movements, we are left with nine constants to represent strain deformation in the element. These

nine constants are to be distributed among the three components of strain ε_x, ε_y and ε_{xy}. As a first-cut, we could assume that the three strain components satisfy:

$$\begin{cases} \varepsilon_x = a_4 + a_5 x + a_6 y \\[2mm] \varepsilon_y = a_7 + a_8 x + a_9 y \\[2mm] \varepsilon_{xy} = a_{10} + a_{11}x + a_{12}y \end{cases} \qquad (2.1.3)$$

We observe that, if the terms of equation (2.1.3) are differentiated, they satisfy the general compatibility equation for strain, namely:

$$\frac{\partial^2 \varepsilon_x}{\partial y^2} + \frac{\partial^2 \varepsilon_y}{\partial x^2} = \frac{\partial^2 \varepsilon_{xy}}{\partial x \partial y} \qquad (2.1.4)$$

Unfortunately, this approach leads to a singular transformation matrix. In an attempt to mitigate the problem, Sabir suggested interpolations for the strain as

$$\begin{cases} \varepsilon_x = a_4 + a_5 y + \left(a_{11}y^2 + 2a_{12}xy^3 \right) \\[2mm] \varepsilon_y = a_6 + a_7 x + \left(-a_{11}x^2 - 2a_{12}x^3 y \right) \\[2mm] \varepsilon_{xy} = a_8 + a_9 x + a_{10}y + \left(a_5 x + a_7 y \right). \end{cases} \qquad (2.1.5)$$

In equations (2.1.5), coefficients a_4, a_6 and a_8 are the terms corresponding to constant strain states. These state ensure convergence as the finite element grid is refined. The terms containing the constants a_5, a_7 and a_9 allow for linear strain behavior. The higher order bracketed terms are added in such a way that

18

the compatibility equations (2.1.4) will be satisfied. Displacement expressions for u and v are obtained by integrating equations (2.1.5), and then adding the rigid body displacements equations (2.1.2). The result is

$$
\begin{cases}
u = a_1 - a_3 y + a_4 x + a_8 y/2 + a_s xy + a_{10} y^2/2 + a_{11} xy^2 + a_{12} x^2 y^3 \\[2mm]
v = a_2 + a_3 y + a_6 y + a_8 x/2 + a_7 xy + a_9 x^2/2 - a_{11} x^2 y - a_{12} x^3 y^2
\end{cases}
\tag{2.1.6}
$$

In matrix form, equation (2.1.6) may be written as

$$
\{u\} = [x]\{A\}
\tag{2.1.7}
$$

where displacements $\{u\} = <u, v>^T$, $\{A\}$ is the parameter matrix $<a_1, a_2, \ldots, a_{12}>^T$, and $[x]$ is the function matrix.

$$
[x] =
\begin{bmatrix}
1 & 0 & -y & x & xy & 0 & 0 & y/2 & 0 & y^2/2 & xy^2 & x^2 y^3 \\[2mm]
0 & 1 & x & 0 & 0 & y & xy & x/2 & x^2/2 & 0 & -x^2 y & -x^3 y^2
\end{bmatrix}
$$

The drilling degree of freedom, Φ, formula is obtained by substituting equations (2.1.6) (i.e. expressions for u and v) into equation (2.0.1),

$$
\Phi = a_3 - \frac{a_5}{2}x + \frac{a_7}{2}y + \frac{a_9}{2}x - \frac{a_{10}}{2}y - 2a_{11}xy - 3a_{12}x^2 y^2
\tag{2.1.8}
$$

Substituting the values of u, v and Φ at each nodes, i.e, $u_i = u(x_i, y_i)$, $v_i = v(x_i, y_i)$ and $\Phi_i = \Phi(x_i, y_i)$ with $i = 1, 2, 3, 4$, into equation (2.1.6) and (2.1.8)

19

gives,

$$\{q\}_{(12\times1)} = [\bar{x}]_{(12\times12)}\{A\}_{(12\times1)}$$

where $\{q\} = <u_1, v_1, \Phi_1, u_2, v_2, \Phi_2, u_3, v_3, \Phi_3, u_4, v_4, \Phi_4>^T$ is nodal parameter vector, and

$$[\bar{x}] = [[\bar{x}_1]^T, [\bar{x}_2]^T, [\bar{x}_3]^T, [\bar{x}_4]^T]^T \qquad (2.1.9)$$

is a (12×12) matrix defined by submatrices $[\bar{x}_i]$ with expressions given by

$$[\bar{x}_i] = \begin{bmatrix} 1 & 0 & -y_i & x_i & x_iy_i & 0 & 0 & y_i/2 & 0 & y_i^2/2 & x_iy_i^2 & x_i^2y_i^3 \\ 0 & 1 & x_i & 0 & 0 & y_i & x_iy_i & x_i/2 & x_i^2/2 & 0 & -x_i^2y_i & -x_i^3y_i^2 \\ 0 & 0 & 1 & 0 & -x_i/2 & 0 & y_i/2 & 0 & x_i/2 & -y_i/2 & -2x_iy_i & -3x_i^2y_i^2 \end{bmatrix}$$

Unlike the naive approximation for displacements, the resulting matrix $[\bar{x}]$ is not singular, and its inverse $[\bar{x}]^{-1}$ can be calculated. So,

$$[A] = [\bar{x}]^{-1}\{q\} \qquad (2.1.10)$$

Substituting equation (2.1.10) into equation (2.1.7) gives

$$u = [x][A] = [x][\bar{x}]^{-1}\{q\} = [N]\{q\} \qquad (2.1.11)$$

where

$$[N] = [x][\bar{x}]^{-1}$$

20

is the matrix of shape functions. Observe that all formulations of finite elements of this kind can be derived by the regular progress of development of finite element formulations, if a inverse of parameter matrix $[\bar{x}]$ exists when the form of the interpolations of displacements, equation (2.1.7), is given by the assumption of the strain field within the entire element.

Even though this membrane component with drilling degree of freedom based on the assumption of the strain states is non-conforming, Sabir [20] and Frey [10] report good numerical performance with quadrilateral elements that are 'close' to being rectangular. Unfortunately, Frey also reports [10] that numerical accuracy of these finite elements is not satisfactory significantly when the same problem are modeled with non-rectangular finite element meshes [20, 10].

2.2 Independent Rotation Interpolation

Flat shell finite elements may be formulated through the use of a variational formulation that includes an independent rotation field for the drilling degree of freedom. The variational formulation is due to Hughes and Brezzi [11, 12]. It employs the skew-symmetric part of the stress tensor as a Lagrange multiplier to enforce the equality of independent rotations with the skew-symmetric part of the displacement gradient. Taylor subsequently combined the variational formulation with an Allman-type interpolation for the displacement field with an independent interpolation field of rotation [14].

2.2.1 Outline of the Variational Formulation

Consider the elastic boundary value problem for a body described by region Ω. The basic equations are:

$$div \ \sigma + f = 0 \qquad (2.2.1)$$

$$skew \ \sigma = 0 \qquad (2.2.2)$$

$$\Phi = skew \ (\nabla \ u) \qquad (2.2.3)$$

$$symm \ \sigma = C \cdot symm \ (\nabla \ u) \qquad (2.2.4)$$

In this family of equations, (2.2.1) represents equilibrium, (2.2.2) the symmetry conditions for stress, (2.2.3) the definition of rotation in terms of displacement gradient, and equation (2.2.4), the constitutive equation. Also, we have

$$\sigma = symm \ \sigma + skew \ \sigma \qquad (2.2.5)$$

$$symm \ \sigma = \frac{1}{2}(\sigma + \sigma^T) \qquad (2.2.6)$$

$$skew \ \sigma = \frac{1}{2}(\sigma - \sigma^T) \qquad (2.2.7)$$

The variational formulation suggested by Hughes and Brezzi [11, 14], can be described as

$$\begin{aligned}
\Pi_\rho(\bar{u}, \bar{\Phi}) \ &= \ \frac{1}{2} \int_\Omega symm(\nabla \ \bar{u}) \cdot C \cdot symm(\nabla \ \bar{u}) d\Omega \\
&+ \frac{1}{2} \ \rho \int_\Omega |skew(\nabla \ \bar{u}) - \bar{\Phi}|^2 d\Omega - \int_\Omega \bar{u} \cdot f d\Omega \qquad (2.2.8)
\end{aligned}$$

where $\bar{u}$ and $\bar{\Phi}$ are trial displacements and rotations on the region Ω, f is the external general forces, and ρ is a penalty. The corresponding variational formulation is

$$
\begin{aligned}
0 &= D\Pi_\rho(u, \Phi)(\bar{u}, \bar{\Phi}) \\
&= \int_\Omega symm(\nabla\ \bar{u}) \cdot C \cdot symm(\nabla\ u) d\Omega \\
&\quad + \rho \int_\Omega [skew(\nabla\ \bar{u}) - \bar{\Phi}]^T [skew(\nabla\ u) - \Phi] d\Omega \\
&\quad - \int_\Omega \bar{u} \cdot f d\Omega \qquad\qquad\qquad\qquad\qquad (2.2.9)
\end{aligned}
$$

2.2.2 Membrane element with drilling degree of freedom

The shell finite element with drilling degree of freedom is derived by combining the Allman-type interpolation for displacement field and the standard bilinear independent rotation field over the entire element [14]. Consider a 4-node quadrilateral element with drilling degree of freedom, as shown in Figure 2.2, where n_{34} is a outward normal direction to the element side $3 - 4$. The independent drilling rotation field is interpolated as a standard bilinear field, i.e,

$$
\Phi = \sum_{i=1}^{4} N_i(\xi, \eta)\Phi_i \qquad\qquad\qquad (2.2.10)
$$

$$
N_i(\xi, \eta) = \frac{1}{4}(1 + \xi_i\xi)(1 + \eta_i\eta); \qquad i = 1, 2, 3, 4
$$
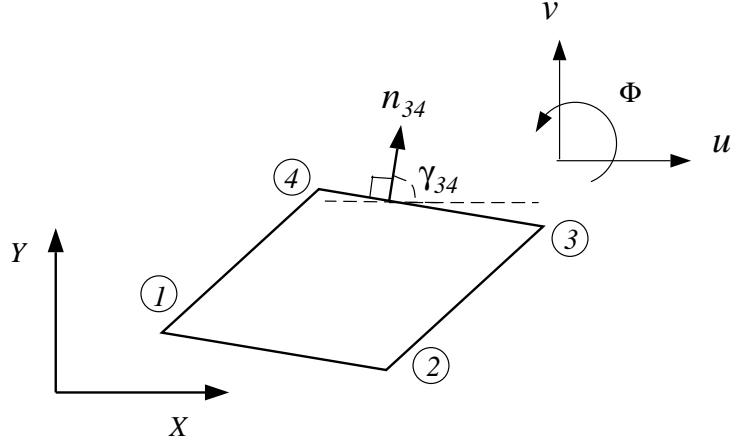
Figure 2.2: A quadrilateral element with drilling degree of freedom.

The Allman-type interpolation for in-plane displacement [4, 1] is

$$
\begin{aligned}
[u] \;=\; & \left\{ \begin{array}{c} u \\ v \end{array} \right\} \\[2ex]
=\; & \sum_{i=1}^{4} N_i(\xi,\eta) \left\{ \begin{array}{c} u_i \\ v_i \end{array} \right\} + \sum_{k=5}^{8} N_k(\xi,\eta) \frac{l_{ij}}{8}(\Phi_j - \Phi_i) \left\{ \begin{array}{c} C_{ij} \\ S_{ij} \end{array} \right\} \quad (2.2.11)
\end{aligned}
$$

where,

$$
\begin{aligned}
x_{ij} \;&=\; x_j - x_i & (2.2.12) \\[1.5ex]
y_{ij} \;&=\; y_j - y_i & (2.2.13) \\[1.5ex]
l_{ij} \;&=\; (x_{ij}^2 + y_{ij}^2)^{\frac{1}{2}} & (2.2.14) \\[1.5ex]
C_{ij} \;&=\; cos\ \gamma_{ij} = \frac{y_{ij}}{l_{ij}} & (2.2.15) \\[1.5ex]
S_{ij} \;&=\; sin\ \gamma_{ij} = -\frac{x_{ij}}{l_{ij}} & (2.2.16)
\end{aligned}
$$

24

$$k \quad = \quad 5, 6, 7, 8 \qquad i, j = 1, 2; 2, 3; 3, 4; 4, 1 \qquad\qquad (2.2.17)$$

$$N_k(\xi, \eta) = \frac{1}{2}(1 - \xi^2)(1 + \eta_k \eta) \qquad k = 5, 7$$

$$N_k(\xi, \eta) = \frac{1}{2}(1 + \xi_k \xi)(1 - \eta^2) \qquad k = 6, 8$$

We further define the matrix notation

$$symm(\nabla \ u) \quad = \quad \left\{ \begin{array}{c} \partial u/\partial x \\ \partial v/\partial y \\ \partial u/\partial y + \partial v/\partial x \end{array} \right\}$$

$$= \quad \sum_{i=1}^{4}([B_i][u_i] + [G_i]\Phi_i) \qquad\qquad (2.2.18)$$

where $[u_i] = \left\{ \begin{array}{c} u_i \\ v_i \end{array} \right\}$ is the nodal translation parameters, and Φ_i is the nodal

drilling degree parameter.

$$[B_i] = \left\{ \begin{array}{cc} \partial N_i/\partial x & 0 \\ 0 & \partial N_i/\partial y \\ \partial N_i/\partial y & \partial N_i/\partial x \end{array} \right\} \qquad\qquad (2.2.19)$$

$$[G_i] = \frac{1}{8} \left\{ \begin{array}{c} l_{ij}C_{ij}\partial N_l/\partial x - l_{ik}C_{ik}\partial N_m/\partial x \\[2ex] l_{ij}S_{ij}\partial N_l/\partial y - l_{ik}S_{ik}\partial N_m/\partial y \\[2ex] (l_{ij}C_{ij}\partial N_l/\partial y - l_{ik}C_{ik}\partial N_m/\partial y) + (l_{ij}S_{ij}\partial N_l/\partial x - l_{ik}S_{ik}\partial N_m/\partial x) \end{array} \right\}$$

$$(2.2.20)$$

When parameter i takes the values $1, 2, 3, 4,$ $\quad m = 5, 6, 7, 8,$ $\quad l = 8, 5, 6, 7,$ $k = 2, 3, 4, 1$ and $j = 4, 1, 2, 3$. Furthermore, we denote

$$skew(\nabla u) - \Phi = \sum_{i=1}^{4}([b_i][u_i] + g_i\Phi_i) \qquad (2.2.21)$$

where,

$$[b_i] = \left\{ -\frac{1}{2}\frac{\partial N_i}{\partial y}, \quad \frac{1}{2}\frac{\partial N_i}{\partial x} \right\} \qquad (2.2.22)$$

$$g_i = -\frac{1}{16}\left(l_{ij}C_{ij}\frac{\partial N_l}{\partial y} - l_{ik}C_{ik}\frac{\partial N_m}{\partial y} \right)$$

$$+\frac{1}{16}\left(l_{ij}S_{ij}\frac{\partial N_l}{\partial x} - l_{ik}S_{ik}\frac{\partial N_m}{\partial x} \right) - N_i \qquad (2.2.23)$$

If we define nodal parameter vector $[q]$ as

$$[q] = \{[q_1], [q_2], [q_3], [q_4]\}^T$$

$$[q_i] = \{u_i, v_i, \Phi_i\}^T \qquad (2.2.24)$$

The first term in the variational equations (2.2.9) produces the element stiffness matrix,

$$[K] = \int_{\Omega} [\bar{B}]^T [C][\bar{B}] d\Omega \qquad (2.2.25)$$

where $[C]$ is the constitutive matrix and

$$[\bar{B}] = \{[\bar{B}_1], [\bar{B}_2], [\bar{B}_3], [\bar{B}_4]\}$$
$$[\bar{B}_i] = \{[B_i], [G_i]\}$$

$[B_i]$ and $[G_i]$ are as defined in equations (2.2.19) and (2.2.20).

The penalty parameter ρ appearing in the second term of equation (2.2.9) is problem dependent [11]. For instance, suppose that the second term in equations (2.2.9) is set to zero — this asserts that the skew-symmetric stresses are zero. It follows that the first term in the equations (2.2.9) expresses equilibrium and the stiffness matrix in equation (2.2.25) is the regular element stiffness matrix without the modification term. In the discrete case, however, skew-symmetric stresses will not be identically zero in general, and thus will play a role in the equilibrium condition [11]. The latter is controlled by the penalty 'ρ'. For isotropic elasticity, it is suggested that ρ may be taken as the shear modulus value [12]. Numerical studies performed by Taylor have shown that the formulation is insensitive to the value of ρ used (at least for several orders of magnitude which bound the shear modulus) [14]. So, we can take the second term in the variational equations (2.2.9) including penalty ρ as the modifica-

tion of the regular element stiffness matrix K for the drilling degree of freedom utilizing independent rotation interpolation field within the element.

From equations (2.2.9) and (2.2.21), the second term in equation (2.2.9) produces modificational term

$$[P] = \rho \int_{\Omega} [\bar{b}]^T \cdot [\bar{b}] d\Omega \qquad (2.2.26)$$

where, ρ is the penalty, $[\bar{b}] = \{[\bar{b}_1], [\bar{b}_2], [\bar{b}_3], [\bar{b}_4]\}$, and $[\bar{b}_i] = \{[b_i], g_i\}$, with $[b_i]$ and g_i defined as in equations (2.2.22) and (2.2.23). Hence, the matrix counterpart of variational equation (2.2.9) for one element is

$$[K^m][q] = [f]$$

where $[f]$ is general external forces, $[q]$ is nodal parameter vector, (defined as (2.2.24)), and $[K^m]$ is final element membrane stiffness matrix with the drilling degree of freedom. The latter is expressed as

$$[K^m] = [K] + [P]$$

where $[K]$ and $[P]$ are given in equations (2.2.25) and (2.2.26).

CHAPTER

3

Plate-Bending Part of Flat Shell Element

The plate bending component of the shell element corresponds to the 12 DOF discrete Kirchhoff quadrilateral (DKQ) plate element, and is derived in detail using the discrete Kirchhoff technique. The DKQ element formulation is based on the discretization of the strain energy. The model neglects the transverse shear strain energy (thin plate). In other words:

$$U = \sum_{e}^{n} U_b^e$$

with

$$U_b^e = \frac{1}{2} \int_{A^e} [\chi]^T [D_b][\chi] dA^e \qquad (3.0.1)$$

Here, U_b^e is the element strain energy due to bending. A^e is the element area.

For a homogeneous isotropic plate $[D_b]$ is given by

$$[D_b] = \frac{Eh^3}{12(1-\nu^2)} \begin{bmatrix} 1 & \nu & 0 \\ \nu & 1 & 0 \\ 0 & 0 & \frac{1}{2}(1-\nu) \end{bmatrix} \tag{3.0.2}$$

where E, ν and h are the Young's modulus, Poisson's ratio and thickness, respectively. The curvature is given by

$$[\chi] = \left\{ \begin{array}{c} -\partial^2 w/\partial x^2 \\ -\partial^2 w/\partial y^2 \\ -2\partial^2 w/\partial x \partial y \end{array} \right\} \tag{3.0.3}$$

where w is transverse displacement.

3.1 Independent Rotation Interpolation

To avoid the difficulty of interpolation of required C^1 continuity, we first assume an interpolation for the independent nodal rotation fields ϑ_x and ϑ_y that describes the rotations of the normal to the undeformed middle surface in the x - y and y -z planes. By definition, θ_x and θ_y are given by

$$\theta_x = \frac{\partial w}{\partial y} = \vartheta_y \tag{3.1.1}$$

$$\theta_y = -\frac{\partial w}{\partial x} = -\vartheta_x \tag{3.1.2}$$

At the middle point of element side, the rotation components along the element sides are eliminated by averaging the corresponding corner nodes values. Rotation components perpendicular to the element sides are assumed to be consistent with a cubic displacement interpolation along the element sides, shown in Figure 3.1. In this derivation, variables i and j are defined as $i, j = 1, 2; 2, 3; 3, 4; 4, 1;$
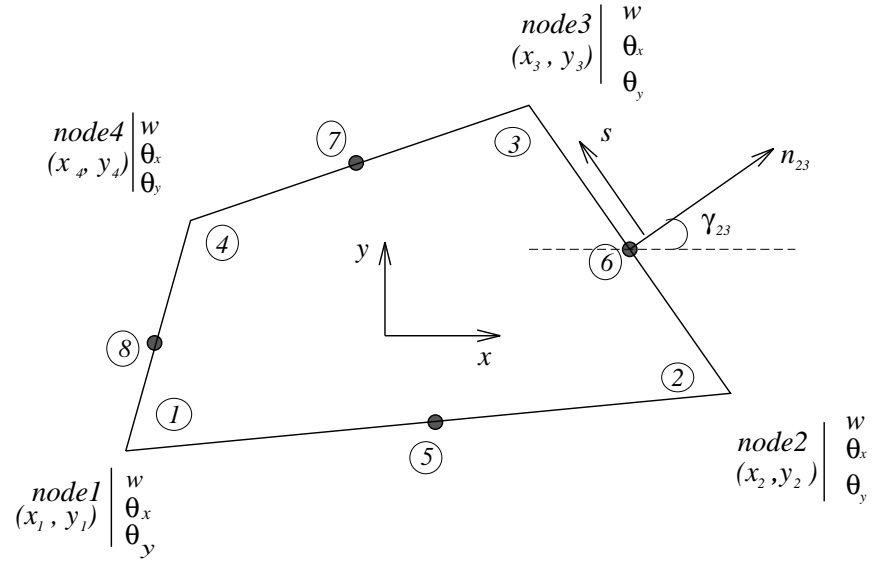
Figure 3.1: 8-node plate bending element.

when $k = 5, 6, 7, 8$, respectively. Therefore, for $\partial w / \partial n|_k$, $\partial w / \partial n$ at mid-side of each side, we can write:

$$\frac{\partial w}{\partial n}|_k = \frac{1}{2} \left(\frac{\partial w}{\partial n}|_i + \frac{\partial w}{\partial n}|_j \right) = \frac{1}{2} \left(\vartheta_{,ni} + \vartheta_{,nj} \right) \tag{3.1.3}$$

for $\partial w / \partial s|_k$, $\partial w / \partial s$ at mid-side of each side, we can assume

$$w = a_1 + a_2 s + a_3 s^2 + a_4 s^3 \tag{3.1.4}$$

31

So,

$$\frac{\partial w}{\partial s} = a_2 + 2a_3 s + 3a_4 s^2 \qquad (3.1.5)$$

Substituting the nodal values into equations (3.1.4) and (3.1.5)

$$w_i = a_1 + a_2 s_i + a_3 s_i^2 + a_4 s_i^3$$

$$\frac{\partial w}{\partial s}\Big|_i = a_2 + 2a_3 s_i + 3a_4 s_i^2$$

$$w_j = a_1 + a_2 s_j + a_3 s_j^2 + a_4 s_j^3$$

$$\frac{\partial w}{\partial s}\Big|_j = a_2 + 2a_3 s_j + 3a_4 s_j^2$$

Generally, we assign

$$s_i = 0;$$

$$s_j = l_{ij} = [(x_j - x_i)^2 + (y_j - y_i)^2]^{1/2}$$

So, we can determine

$$a_2 = \frac{\partial w}{\partial s}\Big|_i$$

$$a_3 = \frac{1}{l_{ij}}\left(-2\frac{\partial w}{\partial s}\Big|_i - \frac{\partial w}{\partial s}\Big|_j + 3\frac{w_j - w_i}{l_{ij}}\right)$$

$$a_4 = \frac{1}{l_{ij}^2}\left(\frac{\partial w}{\partial s}\Big|_i + \frac{\partial w}{\partial s}\Big|_j - 2\frac{w_j - w_i}{l_{ij}}\right)$$

and from equations (3.1.5), I can write

$$\frac{\partial w}{\partial s} = \frac{\partial w}{\partial s}|_i + \frac{2s}{l_{ij}}\left(-2\frac{\partial w}{\partial s}|_i - \frac{\partial w}{\partial s}|_j + 3\frac{w_j - w_i}{l_{ij}}\right)$$

$$+\frac{3s^2}{l_{ij}^2}\left(\frac{\partial w}{\partial s}|_i + \frac{\partial w}{\partial s}|_j - 2\frac{w_j - w_i}{l_{ij}}\right). \tag{3.1.6}$$

At the midpoint of the sides, $s_k = l_{ij}/2$, the $\partial w/\partial s$ expression can be obtained

$$\frac{\partial w}{\partial s}|_k = -\frac{1}{4}\left(\frac{\partial w}{\partial s}|_i + \frac{\partial w}{\partial s}|_j\right) + \frac{3}{2}\left(\frac{w_j - w_i}{l_{ij}}\right)$$

$$= -\frac{1}{4}\left(\vartheta_{,si} + \vartheta_{,sj}\right) + \frac{3}{2}\left(\frac{w_j - w_i}{l_{ij}}\right) \tag{3.1.7}$$

Obviously, from equations (3.1.1) and (3.1.2), we can have

$$[\chi] = \left\{\begin{array}{c} -\partial\vartheta_x/\partial x \\[2mm] -\partial\vartheta_y/\partial y \\[2mm] -\partial\vartheta_x/\partial y - \partial\vartheta_y/\partial x \end{array}\right\} \tag{3.1.8}$$

and define interpolation fields of rotations as incomplete cubic polynomial expression

$$\vartheta_x = \sum_{i=1}^{8} N_i\vartheta_{x_i} \tag{3.1.9}$$

$$\vartheta_y = \sum_{i=1}^{8} N_i\vartheta_{y_i} \tag{3.1.10}$$

33

The shape function $\quad N_i(\xi, \eta)$, where ξ and η are parametric coordinates [27], are those of the 8-node Serendipity element [26].

$$N_i = \frac{1}{2}(1 - \xi^2)(1 + \eta_i \eta), \qquad i = 5, 7$$

$$N_i = \frac{1}{2}(1 - \eta^2)(1 + \xi_i \xi), \qquad i = 6, 8$$

$$N_i = \frac{1}{4}(1 + \xi_i \xi)(1 + \eta_i \eta) - \frac{1}{2}N_m - \frac{1}{2}N_n$$

$$i = 1, 2, 3, 4, \qquad m, n = 8, 5; 5, 6; 6, 7; 7, 8;$$

ϑ_{xi} and ϑ_{yi} are transitory nodal variables affected at the corner and middle-nodes of the quadrilateral element (with straight sides); again, see Figure 3.1.

3.2 Shape Function

The following Kirchhoff assumptions are introduced;

[1] At the corner nodes:

$$\theta_{x_i} = \frac{\partial w}{\partial y}|_i = \vartheta_{y_i} \qquad\qquad (3.2.1)$$

$$\theta_{y_i} = -\frac{\partial w}{\partial x}|_i = -\vartheta_{x_i} \qquad\qquad (3.2.2)$$

$$i = 1, 2, 3, 4$$

[2] At the middle nodes:

$$\frac{\partial w}{\partial s}|_k = \vartheta_{s_k} \qquad\qquad (3.2.3)$$

34

$$\frac{\partial w}{\partial n}\bigg|_k = \vartheta_{n_k} \tag{3.2.4}$$

$$k = 5, 6, 7, 8$$

We note that

[1] w varies independently along the element sides. At the four corner nodes, the nodal variables w appears through the cubic displacement interpolation for the rotation components perpendicular to the element sides (i.e. equation (3.1.7)). w is not defined in the interior of the element.

[2] The Kirchhoff assumptions are satisfied along the entire boundary of the element because $\partial w/\partial s$ and ϑ_s (linear combination of ϑ_x and ϑ_y) are both quadratic expression along the element sides.

[3] Convergence towards the thin plates theory will be obtained for any element length to thickness ratio since the transverse shear energy is neglected. In other words, the DKQ technique is appropriate for thin plates only.

[4] The 12 degree of freedom DKQ elements are such that w, $\partial w/\partial s$, ϑ_x, ϑ_y and $\partial w/\partial n$ are compatible along the element sides.

From geometry we have

$$x_{ij} = x_j - x_i; \qquad y_{ij} = y_j - y_i;$$

$$l_{ij} = (x_{ij}^2 + y_{ij}^2)^{1/2};$$

$$\gamma_{ij} = (x, n_{ij});$$

$$C_k = cos\gamma_{ij} = y_{ij}/l_{ij}; \qquad S_k = sin\gamma_{ij} = -x_{ij}/l_{ij}$$

and

$$\left\{ \begin{array}{c} \vartheta_n \\ \vartheta_s \end{array} \right\} = \left[\begin{array}{cc} C & S \\ -S & C \end{array} \right] \left\{ \begin{array}{c} \vartheta_x \\ \vartheta_y \end{array} \right\} \qquad (3.2.5)$$

$$\left\{ \begin{array}{c} \vartheta_x \\ \vartheta_y \end{array} \right\} = \left[\begin{array}{cc} C & -S \\ S & C \end{array} \right] \left\{ \begin{array}{c} \vartheta_n \\ \vartheta_s \end{array} \right\} \qquad (3.2.6)$$

We now derive an expression that connects the rotational variables at the mid-nodes, ϑ_{x_k} and ϑ_{y_k} ($k = 5, 6, 7, 8$), to terms of the corner nodal variables, w_i, ϑ_{x_i} and ϑ_{y_i} ($i = 1, 2, 3, 4$). It follows from equations (3.2.4) and (3.1.3), and transformation (3.2.5) that

$$\begin{aligned} \vartheta_{n_k} &= \left. \frac{\partial w}{\partial n} \right|_k \\ &= \frac{1}{2} \left(\left. \frac{\partial w}{\partial n} \right|_i + \left. \frac{\partial w}{\partial n} \right|_j \right) \\ &= \frac{1}{2} (\vartheta_{n_i} + \vartheta_{n_j}) \\ &= \frac{1}{2} (C_k \vartheta_{x_i} + S_k \vartheta_{y_i} + C_k \vartheta_{x_j} + S_k \vartheta_{y_j}) \qquad (3.2.7) \end{aligned}$$

Similarly, from equations (3.2.3) and (3.1.7), and transformation (3.2.5), we can write

$$\begin{aligned} \vartheta_{s_k} &= \left. \frac{\partial w}{\partial s} \right|_k \\ &= -\frac{1}{4} \left(\left. \frac{\partial w}{\partial s} \right|_i + \left. \frac{\partial w}{\partial s} \right|_j \right) + \frac{3}{2} \frac{w_j - w_i}{l_{ij}} \end{aligned}$$

36

$$
\begin{aligned}
&= -\frac{1}{4}(\vartheta_{s_i} + \vartheta_{s_j}) + \frac{3}{2}\frac{w_j - w_i}{l_{ij}} \\
&= -\frac{1}{4}(-S_k\vartheta_{x_i} + C_k\vartheta_{y_i} - S_k\vartheta_{x_j} + C_k\vartheta_{y_j}) + \frac{3}{2}\frac{w_j - w_i}{l_{ij}}
\end{aligned}
\tag{3.2.8}
$$

$$
k = 5, 6, 7, 8, \qquad i,j = 1,2; 2,3; 3,4; 4,1;
$$

From above equations (3.2.7) and (3.2.8), and transformation (3.2.6), as well I can write

$$
\begin{aligned}
\vartheta_{x_k} &= C_k\vartheta_{n_k} - S_k\vartheta_{s_k} \\
&= (\frac{1}{2}C_k^2 - \frac{1}{4}S_k^2)\vartheta_{x_i} + \frac{3}{4}C_kS_k\vartheta_{y_i} + (\frac{1}{2}C_k^2 - \frac{1}{4}S_k^2)\vartheta_{x_j} \\
&\quad + \frac{3}{4}C_kS_k\vartheta_{y_j} - \frac{3}{2}S_k\frac{w_j - w_i}{l_{ij}}
\end{aligned}
\tag{3.2.9}
$$

and

$$
\begin{aligned}
\vartheta_{y_k} &= S_k\vartheta_{n_k} + C_k\vartheta_{s_k} \\
&= \frac{3}{4}C_kS_k\vartheta_{x_i} + (\frac{1}{2}S_k^2 - \frac{1}{4}C_k^2)\vartheta_{y_i} + \frac{3}{4}C_kS_k\vartheta_{x_j} \\
&\quad + (\frac{1}{2}S_k^2 - \frac{1}{4}C_k^2)\vartheta_{y_j} + \frac{3}{2}C_k\frac{w_j - w_i}{l_{ij}}
\end{aligned}
\tag{3.2.10}
$$

Using (3.2.1) and (3.2.2), by defining

$$
\begin{aligned}
a_k &= \frac{3}{4}C_kS_k = -\frac{3}{4}\frac{x_{ij}y_{ij}}{l_{ij}^2} \\
b_k &= \frac{1}{2}C_k^2 - \frac{1}{4}S_k^2 = (\frac{1}{2}y_{ij}^2 - \frac{1}{4}x_{ij}^2)/l_{ij}^2 \\
c_k &= \frac{S_k}{l_{ij}} = -\frac{x_{ij}}{l_{ij}}^2
\end{aligned}
\tag{3.2.11}
$$

37

$$d_k = \frac{1}{2}S_k^2 - \frac{1}{4}C_k^2 = (\frac{1}{2}x_{ij}^2 - \frac{1}{4}y_{ij}^2)/l_{ij}^2$$

$$e_k = -\frac{C_k}{l_{ij}} = -\frac{y_{ij}}{l_{ij}}^2$$

Now we can rewrite (3.2.9) and (3.2.10), as

$$
\begin{aligned}
\vartheta_{x_k} &= \frac{3}{4}C_k S_k \theta_{x_i} - (\frac{1}{2}C_k^2 - \frac{1}{4}S_k^2)\theta_{y_i} \\
&\quad + \frac{3}{4}C_k S_k \theta_{x_j} - (\frac{1}{2}C_k^2 - \frac{1}{4}S_k^2)\theta_{y_j} - \frac{3}{2}S_k \frac{w_j - w_i}{l_{ij}} \\
&= a_k \theta_{x_i} - b_k \theta_{y_i} + a_k \theta_{x_j} - b_k \theta_{y_j} - \frac{3}{2}c_k(w_j - w_i) \qquad (3.2.12)
\end{aligned}
$$

$$
\begin{aligned}
\vartheta_{y_k} &= (\frac{1}{2}S_k^2 - \frac{1}{4}C_k^2)\theta_{x_i} - \frac{3}{4}C_k S_k \theta_{y_i} \\
&\quad + (\frac{1}{2}S_k^2 - \frac{1}{4}C_k^2)\theta_{x_j} - \frac{3}{4}C_k S_k \theta_{y_j} + \frac{3}{2}C_k \frac{w_j - w_i}{l_{ij}} \\
&= d_k \theta_{x_i} - a_k \theta_{y_i} + d_k \theta_{x_j} - a_k \theta_{y_j} - \frac{3}{2}e_k(w_j - w_i) \qquad (3.2.13)
\end{aligned}
$$

Explicit expressions of the rotations ϑ_x and ϑ_y of a general quadrilateral in terms of the final nodal variables,

$$\{q\} = \langle w_1, \theta_{x_1}, \theta_{y_1}, w_2, \theta_{x_2}, \theta_{y_2}, w_3, \theta_{x_3}, \theta_{y_3}, w_4, \theta_{x_4}, \theta_{y_4} \rangle^T \qquad (3.2.14)$$

are obtained by substituting (3.2.12) and (3.2.13) ($k = 5, 6, 7, 8 \quad i, j = 1, 2; 2, 3; 3, 4; 4, 1$) into (3.1.9) and (3.1.10). This gives

$$\vartheta_x = \sum_{i=1}^{8} N_i \vartheta_{x_i}$$

$$
\begin{aligned}
&= \sum_{i=1}^{4}(-N_i)\theta_{y_i} + \sum_{k=5}^{8}N_k\vartheta_{x_k} \\
&= -\sum_{i=1}^{4}N_i\theta_{y_i} + \sum_{k=5}^{8}N_k[a_k\theta_{x_i} - b_k\theta_{y_i} + a_k\theta_{x_j} - b_k\theta_{y_j} - \frac{3}{2}c_k(w_j - w_i)] \\
&= \langle H^x(\xi,\eta)\rangle\{q\} && (3.2.15)
\end{aligned}
$$

and

$$
\begin{aligned}
\vartheta_y &= \sum_{i=1}^{8}N_i\vartheta_{y_i} \\
&= \sum_{i=1}^{4}N_i\theta_{x_i} + \sum_{k=5}^{8}N_k\vartheta_{y_k} \\
&= \sum_{i=1}^{4}N_i\theta_{x_i} + \sum_{k=5}^{8}N_k[d_k\theta_{x_i} - a_k\theta_{y_i} + d_k\theta_{x_j} - a_k\theta_{y_j} - \frac{3}{2}e_k(w_j - w_i)] \\
&= \langle H^y(\xi,\eta)\rangle\{q\} && (3.2.16)
\end{aligned}
$$

where $\langle H^x(\xi,\eta)\rangle$ and $\langle H^y(\xi,\eta)\rangle$ are the shape functions. In component form, the shape functions are

$$
\langle H^x(\xi,\eta)\rangle = \langle H_1^x, H_2^x, \dots, H_{12}^x\rangle, \qquad (3.2.17)
$$

and

$$
\langle H^y(\xi,\eta)\rangle = \langle H_1^y, H_2^y, \dots, H_{12}^y\rangle, \qquad (3.2.18)
$$

with

$$H_1^x = \tfrac{3}{2}(c_5 N_5 - c_8 N_8); \qquad H_1^y = \tfrac{3}{2}(e_5 N_5 - e_8 N_8)$$

$$H_2^x = a_5 N_5 + a_8 N_8; \qquad H_2^y = N_1 + d_5 N_5 + d_8 N_8$$

$$H_3^x = -N_1 - b_5 N_5 - b_8 N_8; \qquad H_3^y = -a_5 N_5 - a_8 N_8 = -H_2^x$$

$$H_4^x = \tfrac{3}{2}(c_6 N_6 - c_5 N_5); \qquad H_4^y = \tfrac{3}{2}(e_6 N_6 - e_5 N_5)$$

$$H_5^x = a_6 N_6 + a_5 N_5; \qquad H_5^y = N_2 + d_6 N_6 + d_5 N_5$$

$$H_6^x = -N_2 - b_6 N_6 - b_5 N_5; \qquad H_6^y = -a_6 N_6 - a_5 N_5 = -H_5^x$$

$$H_7^x = \tfrac{3}{2}(c_7 N_7 - c_6 N_6); \qquad H_7^y = \tfrac{3}{2}(e_7 N_7 - e_6 N_6)$$

$$H_8^x = a_7 N_7 + a_6 N_6; \qquad H_8^y = N_3 + d_7 N_7 + d_6 N_6$$

$$H_9^x = -N_3 - b_7 N_7 - b_6 N_6; \qquad H_9^y = -a_7 N_7 - a_6 N_6 = -H_8^x$$

$$H_{10}^x = \tfrac{3}{2}(c_8 N_8 - c_7 N_7); \qquad H_{10}^y = \tfrac{3}{2}(e_8 N_8 - e_7 N_7)$$

$$H_{11}^x = a_8 N_8 + a_7 N_7; \qquad H_{11}^y = N_4 + d_8 N_8 + d_7 N_7$$

$$H_{12}^x = -N_4 - b_8 N_8 - b_7 N_7; \qquad H_{12}^y = -a_8 N_8 - a_7 N_7 = -H_{11}^x$$

$$(3.2.19)$$

CHAPTER

4

Numerical Examples

Performance of the flat shell finite elements is evaluated by working through four numerical examples. They are:

(a) Shear-loaded cantilever beam,

(b) Square plate simply supported on four edges,

(c) Cantilever I-shape cross section beam, and

(d) Folded plate simply supported on two opposite sides.

Applications (a) and (c) have been selected because they are simple enough for analytical solutions to exist, and because they produce displacements in the drilling degree of freedom. Application (b) is a standard problem from plate analysis.

In case studies (a)-(d), performance of the flat shell finite element is compared to a four node flat shell element in ANSYS-5.0, which has six degrees of freedom per node, and includes a drilling degree of freedom based on an approach suggested by Kanok-Nukulchai [18]. Unlike the flat shell element presented in this thesis, Kanok-Nukulchai uses a degeneration concept, in which the displacements and rotations of the shell mid-surface are independent variables. Bilinear functions are employed in conjunction with a reduced integration

for the transverse shear energy. The result is a so-called bilinear degenerated shell element. Application (c) is also computed using a quadrilateral flat shell element (six degrees of freedom per node) from SAP-90.

4.1 Shear-loaded cantilever beam

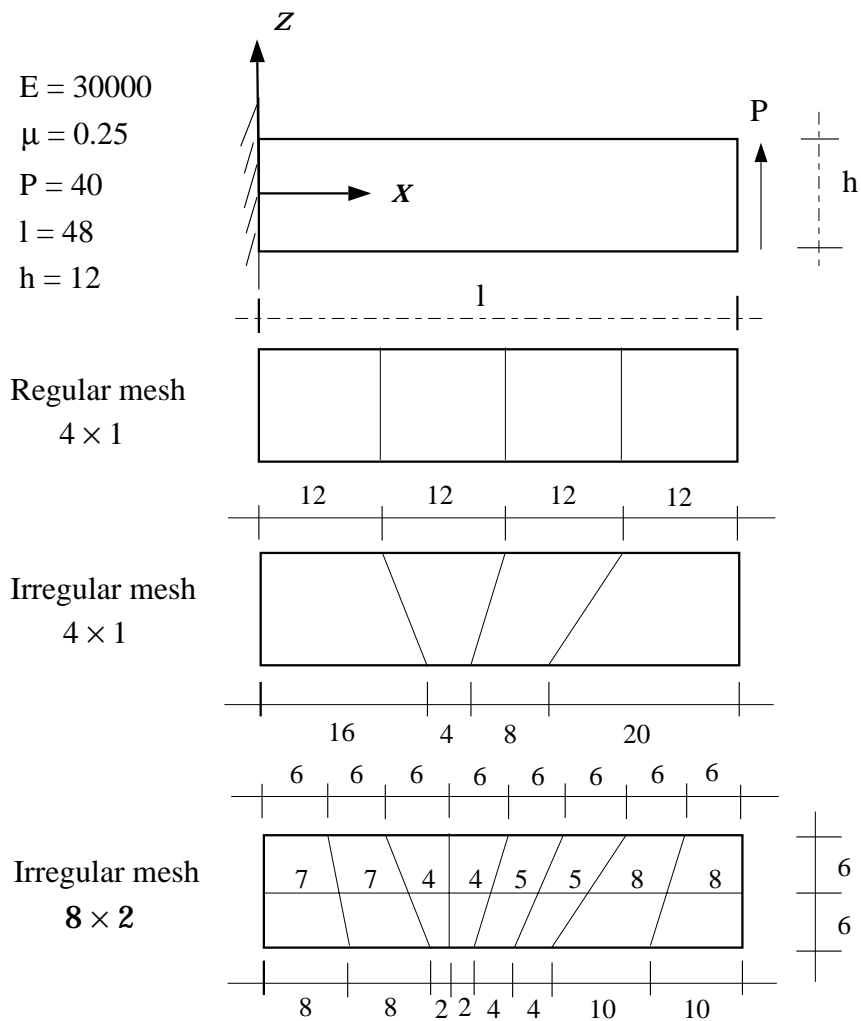A shear-loaded cantilever beam, as shown in Figure 4.1, has been used as a test

Figure 4.1: Meshes of a short cantilever beam.

problem by many authors [2, 14, 20]. In this study finite element solutions are computed for a mesh of four square elements, finer meshes constructed by bisection, and also for a irregular meshes of four and sixteen quadrilateral elements. From elasticity [13, 23], the analytical solution for the tip displacement is

$$w = \frac{Pl^3}{3EI} + \frac{(4 + 5\mu)Pl}{2Eh}.\tag{4.1.1}$$

Substituting the material and section properties selected in Figure 4.1 into equation (4.1.1) gives $w = 0.3553$. The numerical results for this shell finite element are compared against the theoretical solution, and numerical results reported in the literature for the performance of other elements. Table 4.1 contains a summary of numerical results, with the asterisk (*) denoting the irregular mesh. The Sabir element is a rectangular element with the drilling degree of freedom, the Allman element is a rectangular element with the vertex rotation and the bilinear element is a rectangular constant strain element without any nodal rotational degree of freedom.

The numerical results from this test problem indicate that, with the same regular meshes, the shell finite element described in this thesis gives more accurate results than other shell finite elements in the literature. For the same irregularly shaped meshes, the present shell element provides much greater accuracy than ANSYS-5.0. The numerical results also suggest that the shell element described herein gives reasonably accurate and rapidly convergent results with distorted meshes.

Meshes	4×1	8×2	16×4	$4 \times 1^*$	$8 \times 2^*$
Present element	0.3445	0.3504	0.3543	0.3066	0.3455
Error to theoretical solution	3.039%	1.379%	0.282%	13.707%	2.758%
ANSYS–5.0	0.2424	0.3162	0.3449	0.2126	0.2996
Sabir [20]	0.3281	0.3454	0.3527	——	——
Allman [2]	0.3026	0.3394	0.3512	——	——
Bilinear element	0.2424	0.3162	0.3447	——	——

Table 4.1: Comparison in some results of the tip displacement, w, for the short cantilever beam.

4.2 Square Plate Simply Supported on Four Edges

Consider the square plate simply supported on four edges, as shown in Figure 4.2. Two load cases are considered; (a) a uniform loading over the entire plate, and (b) a concentrated point load at the center of the plate. For each load case, computed displacements are compared to analytical displacements.

4.2.1 Uniform Loading over the Entire Plate

Consider a square plate simply supported on all four edges subjected to a uniforming loading, shown in Figure 4.2. The exact transverse displacement at the center, w_c^*, from the plate theory [7, 24] can be expressed as

$$w_c^* = 0.00406 \frac{q_0 a^4}{D} \qquad (4.2.1)$$

44

$\text{E} = 10^7 \text{psi}$

$\boldsymbol{\mu} = 0.3$

$\text{h} = 0.5"$

$\text{q}_0 = 300 \text{ psi}$

$\text{a} = 10"$

Figure 4.2: Meshes of square plate simply supported on 4 edges.

where q_0 is the uniforming loading, a is the length of edge of the square plate and

$$D = \frac{Eh^3}{12(1 - \mu^2)} \tag{4.2.2}$$

Substituting the values of E, μ, h, q_0 and a of this example into equations (4.2.1) and (4.2.2) gives

$$D = 1.1446886 \times 10^5$$

and

$$w_c^* = 1.064045 \times 10^{-1}(in).$$

Because the plate geometry is symmetric about x-axis and y-axis, only one quarter of the plate is taken for numerical computation. Regular meshes on the

45

plate quarter with $N = 2$ and 4 (See Figure 4.2) are considered. Numerical results are evaluated by comparing the transverse displacements of the plate center, w_c, to the exact theoretical solution. A summary of results is provided in Table 4.2. Once again, the present element generates displacements that are closer to the theoretical solution than predicted by the shell element from ANSYS-5.0.

Meshes N	2	4
Displacements w_c $(\times 10^{-1})$	1.06027	1.06405
Error to theoretical solution	0.355%	0.000489%
ANSYS–5.0 w_c $(\times 10^{-1})$	1.0044	1.0492

Table 4.2: The transverse displacements at the center of the square plate simply supported on 4 edges under uniform load over the entire plate with different meshes and the comparations with the exact theoretical solution.

4.2.2 Concentrated Loading at the Center

Similarly, consider the square plate subjected to a concentrated loading, $P = 30000bl$ at the center. The theoretical exact transverse displacement at the center, w_c^*, from the plate theory [7, 24], can be expressed as
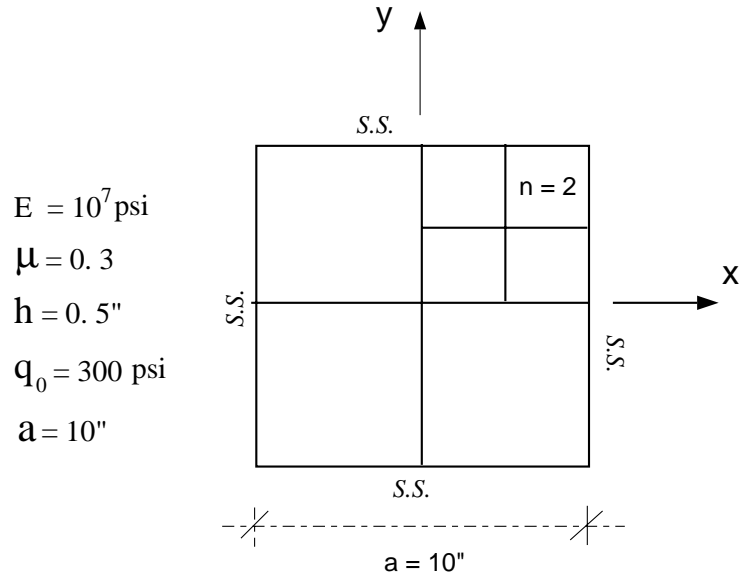
$$w_c^* = 0.0115999 \frac{Pa^2}{D} \tag{4.2.3}$$

where P is the concentrated loading at the center, a is the length of edge of the square plate, and D is as described in equation (4.2.2). Substituting the values

of D, P, and a into equation (4.2.3) gives

$$w_c^* = 3.0401019 \times 10^{-1}(in) \tag{4.2.4}$$

Once again, numerical displacements are computed for only a quarter of the plate. With regular meshes $N = 2$, 4 and 8 (See Figure 4.2), the transverse displacements at the center w_c computed by the elements described in this thesis are compared with the exact theoretical solution in Table 4.3.

Meshes N	2	4	8
Displacements w_c $(\times 10^{-1})$	3.32666	3.12850	3.06664
Error to theoretical solution	9.426%	2.908%	0.873%
ANSYS–5.0 w_c $(\times 10^{-1})$	3.1574	3.0777	3.0518

Table 4.3: The transverse displacements at the center of the square plate simply supported on 4 edges under concentrated point load at the center with different meshes and the comparations with the exact theoretical solution.

4.3 Cantilever I-shape Cross Section Beam

In the third example, displacements are computed for a cantilever beam having an I-shape cross section. Three load cases are considered. The first is displacements due to a concentrated load at the center of the free end, as shown in Figure 4.3. Second, displacements are computed for a uniform load on the center line of the top face, as shown in Figure 4.4. The third is under two level concentrated loads at the flanges of the free end in opposite directions along y, as shown in

Figure 4.5. The numerical solutions of these three cases for all meshes are also computed using commercial finite element tools, ANSYS-5.0 and SAP-90, and contained in the corresponding tables.

4.3.1 Concentrated Load at the Center of the Free End

Displacements are computed for a cantilever beam with I-shape cross section loaded with point load P at the center of the free end shown in Figure 4.3. The solution of the transverse displacement at the free end, w^*, from the beam

$E = 10^7 psi$
$\mu = 0.3$
$t = 0.25''$
$L = 40''$
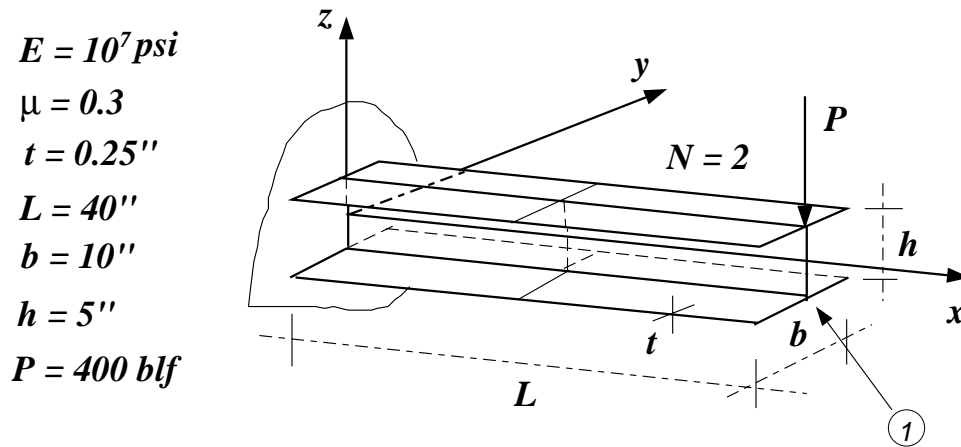$b = 10''$
$h = 5''$
$P = 400 \, blf$

Figure 4.3: Cantilever I-beam under a concentrated load at the end.

bending theory with shear effect is expressed as

$$w^* = \frac{PL^3}{3EI} + \frac{PL}{A_w G} \tag{4.3.1}$$

48

where the second term represents shear effect. P is the load, and L is the length of the beam. $I = 33.8802$ is modulus of the area and $A_w = 1.1875$ is area of the web. Suppose that the shear modulus is as $E/G = 2.5$. Substitute values of I, A_w, E, G, P and L into equation (4.3.1), so that

$$w^* = 2.85552 \times 10^{-2}(in)$$

The transverse displacements w at point 1 (see Figure 4.3) are computed by using the elements described in this thesis. Results are tabulated in Table 4.4. Speed of convergence for numerical results is define. The convergent rate λ

$$\lambda_{N_i} = \frac{w_{N_i} - w_{N_{i-1}}}{w_{N_i}},$$

with $N_1 = 1$, $N_2 = 2$, $N_3 = 4$, $N_4 = 8$ and $N_5 = 16$ describes the rate of convergence for numerical results. These results are tabulated in the same table. We can observe that the displacement computed with $N = 8$ is already very closed to the result from the beam bending theory.

4.3.2 Uniform Load along Center Line of Top Face

Also, I look at a cantilever beam with I-shape cross section under a uniformly distributed line load q_0 along the center line of the top face, as shown in Figure 4.4. The solution of the transverse displacement at the free end, w^*, from the

Meshes N	2	4	8	16
Displacement w ($\times 10^{-2}$)	-2.65646	-2.80859	-2.85107	-2.85482
ANSYS–5.0 w ($\times 10^{-2}$)	-1.9158	-2.5457	-2.7789	-2.8424
SAP–90 w ($\times 10^{-2}$)	-2.2862	-2.6772	-2.8150	-2.8486

Table 4.4: The transverse displacements at the free end of the I-shape section cantilever beam under concentrated point load at the center of the free end with different meshes and their convergent rates.

beam bending theory with shear effect is expressed as

$$w^* = \frac{q_0 L^4}{8EI} + \frac{q_0 L^2}{2A_w G} \tag{4.3.2}$$

where similarly the second term represents shear effect. q_0 is the unique load, and L is the length of the beam. Substituting $q_0 = 20bl/in$, $L = 40$", $I = 33.8802$, $A_w = 1.1875$ and $E/G = 2.5$ into equation (4.3.2) produces

$$w^* = 2.22585 \times 10^{-2}$$

The transverse displacements w at point 1 (see Figure 4.4) computed by using the elements described in this thesis; convergent rates are tabulated in Table 4.5.

From the two cases of the I-beam above, we can see that the displacements from beam bending theory and computed by elements in this thesis are in very close agreement.
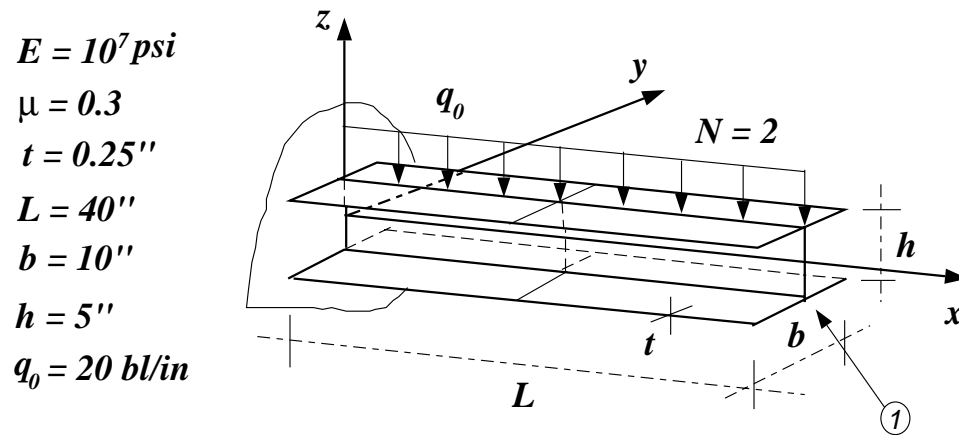
$E = 10^7 psi$
$\mu = 0.3$
$t = 0.25''$
$L = 40''$
$b = 10''$
$h = 5''$
$q_0 = 20\ bl/in$

Figure 4.4: Cantilever I-beam under a uniformly distributed line load along the center line of the top face.

4.3.3 Two Level Concentrated Loads at the Flanges of the Free End in Opposite Directions Along y

Displacements are computed for a cantilever beam having I-shape cross section, subject to two concentrated load P at the flanges of the free end in opposite directions along y, as shown in Figure 4.5. The transverse displacements w at point 1 (see Figure 4.5) are computed by using the elements described in this thesis and their convergent rates are tabulated in Table 4.6.

The horizontal displacements along y, v, at point 1 (see Figure 4.5) computed by using the elements described in this thesis and their convergent rates are tabulated in Table 4.7.

51

Meshes N	2	4	8	16
Displacement w $(\times 10^{-2})$	-2.19184	-2.22248	-2.23926	-2.24607
ANSYS–5.0 w $(\times 10^{-2})$	-1.6003	-2.0237	-2.1862	-2.2339
SAP–90 w $(\times 10^{-2})$	-2.0861	-2.1831	-2.2228	-2.2413

Table 4.5: The transverse displacements at the free end of the I-shape section cantilever beam under uniform load along center line of the top face with different meshes and their convergent rates.

Meshes N	2	4	8	16
Displacement w $(\times 10^{-1})$	2.45142	2.50528	2.51482	2.52135
ANSYS–5.0 w $(\times 10^{-1})$	1.1280	1.8943	2.3378	2.5135
SAP–90 w $(\times 10^{-1})$	2.0218	2.3010	2.4562	2.5195

Table 4.6: The transverse displacements at point 1 of the I-shape section cantilever beam under two lever concentrated loads at the flanges of the free end in opposite directions along y with different meshes and their convergent rates.

4.4 Folded Plate Simply supported on two opposite sides

As the third example, I consider a folded plate, as shown in Figure 4.6. The meshes with $N = 1$, 2 and 4 are used and the results, the transverse displacements w at points 1 and 2, and their convergent rates λ are tabulated in Table 4.8 and Table 4.9, respectively.

From the examples of the I-beam and the folded plate, it can be observed that the solutions rapidly converge, and are stable.
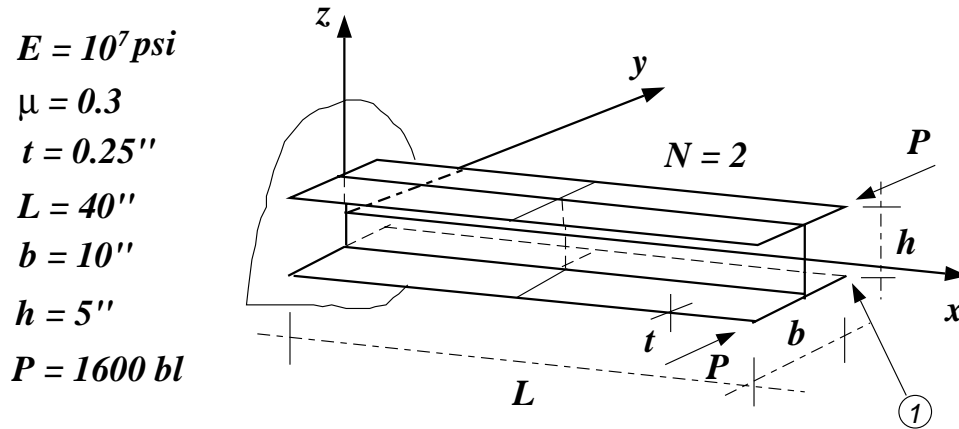
$E = 10^7 psi$
$\mu = 0.3$
$t = 0.25''$
$L = 40''$
$b = 10''$
$h = 5''$
$P = 1600\ bl$

Figure 4.5: Cantilever I-beam under two level concentrated loads at the flanges of the free end in opposite directions along y.

Meshes N	2	4	8	16
Displacement v $(\times 10^{-1})$	1.38753	1.46572	1.48824	1.49583
ANSYS–5.0 v $(\times 10^{-1})$	0.6299	1.1112	1.3743	1.4601
SAP–90 v $(\times 10^{-1})$	1.0434	1.3116	1.4407	1.4833

Table 4.7: The horizontal displacements at point 1 of the I-shape section cantilever beam under two lever concentrated loads at the flanges of the free end in opposite directions along y with different meshes and their convergent rates.
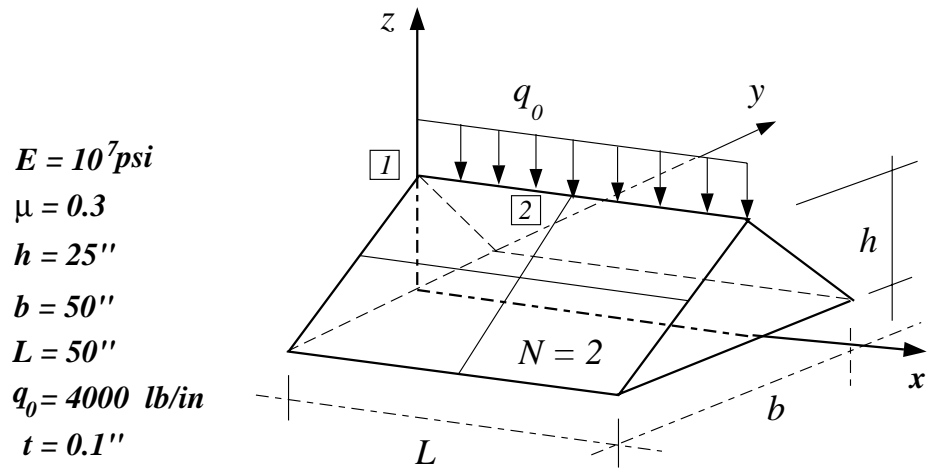
Figure 4.6: A folded plate simply supported on two opposite sides.

Meshes N	1	2	4
Displacement w $(\times 10^{-1})$	-1.38009	-1.41003	-1.42237
ANSYS–5.0 w $(\times 10^{-1})$	-1.3654	-1.4068	-1.4209

Table 4.8: The transverse displacements at point 1 of the folded plate simply supported on two opposite sides under uniform load along the center line with different meshes and their convergent rates.

Meshes N	1	2	4
Displacement w $(\times 10^{-1})$		-1.35207	-1.36062
ANSYS–5.0 w $(\times 10^{-1})$		-1.3514	-1.3604

Table 4.9: The transverse displacements at point 2 of the folded plate simply supported on two opposite sides under uniform load along the center line with different meshes and their convergent rates.

CHAPTER
5

Conclusions and Future Work

This thesis has presented the formulation of a four-node thin flat shell finite element. The shell finite element is the combination of a membrane element, with the drilling degrees of freedom, and a discrete Kirchhoff plate finite element. As mentioned in Chapter 2, the drilling degree of freedom may be introduced into the membrane element in more than one way. In this project we have introduced the drilling degree of freedom via a variational formulation. The variational formulation employs enforcement of equality of the independent rotation field and skew-symmetric part of the displacement gradient.

Numerical experiments have been conducted to assess the accuracy and reliability of the shell element, compared to theoretical results (when available), and other shell finite elements. The flat shell elements shows excellent performance for both regular and distorted meshes.

Future work will include the formulation of a mass matrix for the flat shell finite element. The mass matrix is needed for dynamic analyses; it can be computed in at least two ways. The easiest approach is to simply form the lumped mass matrix. A second method is to form the consistent mass matrix by integrating the shape functions. One advantage of the second approach is mass

matrices that are nonsingular, and hence dynamic analyses involving eigenvalue computations may be done without the additional steps of sub-structuring.

BIBLIOGRAPHY

[1] Allman D. J., "A Compatible Triangular Element Including Vertex Rotations for Plane Elasticity Analysis", *Computers and Structures*, Vol. 19, 1984, pp 1-8.

[2] Allman D. J., "A Quadrilateral Finite Element Including Vertex Rotations for Plane Elasticity Analysis", *International Journal for Numerical Methods in Engineering*, Vol. 26, 1988, pp 717-730.

[3] Allman D. J., "Evaluation of the Constant Strain Triangle with Drilling Rotations", *International Journal for Numerical Methods in Engineering*, Vol. 26, 1988, pp 2645-2655.

[4] Allman D. J., "The Constant Strain Triangle with Drilling Rotations: A Simple Prospect for Shell Analysis", *Mathematics of Finite Elements and Applications VI (MAFELAP 1987)*, J. R. Whiteman (ed.), Academic Press, New York, 1988, pp 233-240.

[5] Baumann M., Schweizerhof K. and Andrussow S., " An Efficient Mixed Hybrid 4-Node Shell Element with Assumed Stresses for Membrane, Bending and Shear Parts", *Engineering Computations*, Vol. 11, 1994, pp 69-80.

[6] Bergan P. G. and Felippa C. A., " A Triangular Membrane Element with Rotational Degrees of Freedom", *Computer Methods in Applied Mechanics and Engineering*, Vol. 50, 1985, pp 25-69.

[7] Chang P., " Class Notes of Theory of Plates and Shells", *University of Maryland at College Park*, Department of Civil Engineering, Fall, 1993.

[8] Ciarlet P. G., " Conforming Finite Element Method for Shell Problem", *Mathematics of Finite Elements and Applications II*, J. R. Whiteman (ed.), Academic Press, London, 1977.

[9] Cook R. D., " On the Allman Triangle and a Related Quadrilateral Element", *Computers and Structures*, Vol. 22, 1986, pp 1065-1067.

[10] Frey F., " Shell Finite Elements with Six Degrees of Freedom per Node", *Analytical and Computational Models of Shell*, CED-Vol. 3, pp 291-316.

[11] Hughes T. J. R., " On Drilling Degrees of Freedom", *Computer Methods in Applied Mechanics and Engineering*, Vol. 72, 1989, pp 105-121.

[12] Hughes T. J. R., Brezzi F., Masud A. and Harari I., " Finite Elements with Drilling Degrees of Freedom: Theory and Numerical Evaluations", *Proceedings of the Fifth International Symposium on Numerical Methods in Engineering*, Computational Mechanics Publications, Ashurst, U.K., 1989, pp 3-17.

[13] Hughes T. J. R., " The Finite Elements Methods: Linear Static and Dynamic Finite Element Analysis", Prentice-Hall, Englewood Cliffs, New Jersey, 1987.

[14] Ibrahimbegovic A., Taylor R. L. and Wilson E. L., " A Robust Quadrilateral Membrane Finite Element with Drilling Degrees of Freedom", *International Journal for Numerical Methods in Engineering*, Vol. 30, 1990, pp 445-457.

[15] Ibrahimbegovic A. and Wilson E. L., " A Unified Formulation for Triangular and Quadrilateral Flat Shell Finite Element with Six Nodal Degrees of

Freedom", *Communications in Applied Numerical Methods*, Vol. 7, 1991, pp 1-9.

[16] Jaamei S. and Frey F., " A Thin Shell Finite Element with Drilling Rotations", *Proceedings of the Fifth International Symposium on Numerical methods in Engineering, September, 1989,* " Computational mechanics Publications, Ashurst, U.K.", 1989, pp 425-430.

[17] Jean-Louis Batoz and Mabrouk Ben Tahar, " Evaluation of a New Quadrilateral Thin Plate Bending Element", *International Journal for Numerical Methods in Engineering*, Vol. 18, 1982, pp 1655-1677.

[18] Kanok-Nukulchai, " A Simple and Efficient Finite Element for General Shell Analysis", *International Journal for Numerical Methods in Engineering*, Vol. 14, 1979, pp 179-200.

[19] Macneal R. H. and Harder R. L., " A refined Four-nodes membrane Element with Rotational Degrees of freedom", *computers and Structures*, Vol. 28, 1988, pp 75-84.

[20] Sabir A. B., " A Rectangular and a Triangular Plane Elasticity Element with Drilling Degrees of Freedom", *Proceedings of the Second International Conference on Variational Methods in Engineering,* " Brebbia C. A. (ed.), Southampton University, July, 1985, Springer-Verlag, berlin", 1985, pp 17-25.

[21] Taig I. C. and Kerr R. I., " Some Problems in the Discrete Element Representation of Aircraft Structures ", *Matrix Methods of Structural Analysis ,* " Veubeke (ed.), Pergamon Press, London", 1964.

[22] Taylor R. L., " Finite Element Analysis of Linear Shell Problems ", *Mathematics of Finite Elements and Applications VI (MAFELAP 1987),* " Whiteman J. R. (ed.), Academic Press, New York", 1988, pp 191-203.

[23] Timoshenko S. and Goodier J. N., " Theory of Elasticity", McGraw-Hill, New York, 1951.

[24] Timoshenko S. and Woinowsky-Krieger S., " Theory of Plates and Shells", *Second Edition*, McGraw-Hill, New York, 1959.

[25] Turner M. J., Clough R. W., Martin H. C. and Topp L. J., " Stiffness and Deflection Analysis of Complex Structures ", *Journal for Aerospace Science* , Vol. 23, 1956.

[26] Zienkiewicz O. C. and Taylor R. L., " The Finite Element Method", *Fourth Edition*, Vol. 2.

[27] Zienkiewicz O. C., " The Finite Element Method", *Third Expanded and Revised Edition*, McGraw-Hill, U.K. 1977.